Solar Spectral Irradiance under Clear and Cloudy Skies: Measurements and a Semiempirical Model

STEFAN NANN

Centre for Solar Energy and Hydrogen Research, Stuttgart, Federal Republic of Germany

CAROL RIORDAN

Solar Energy Research Institute, Golden, Colorado

(Manuscript received 19 June 1990, in final form 8 October 1990)

ABSTRACT

In a combined effort, the Centre for Solar Energy and Hydrogen Research in Germany and the Solar Energy Research Institute in the United States analyzed several thousand measurements of the solar spectral irradiance recorded at four sites. The goal was to develop a semiempirical model that describes the total solar spectral irradiance for clear and cloudy sky conditions based on readily available input data.

To investigate how the spectral transmission of clouds deviates from an assumed neutral density filter, the measured spectra are compared with simulated clear-sky spectra. A correlation is established between the cloud thickness and the relatively higher transmission of clouds in the ultraviolet and blue region of the solar spectrum. Using this approach, a semiempirical model is proposed based solely on global and diffuse broadband irradiance measurements, precipitable water-vapor data, and the sun's position. The model, called SEDES1, is applied to calculate spectral irradiance in short time steps (30 or 60 minutes) that are needed for either the design and performance analysis of spectrally selective solar energy conversion systems or to predict daylight availability. The results are also applicable to current climate research areas such as validating radiative transfer codes.

1. Introduction

The natural variation of spectral solar radiation at the earth's surface is being investigated in a combined effort at the Centre for Solar Energy and Hydrogen Research (ZSW) in Germany and the Solar Energy Research Institute (SERI) in the United States as a part of their solar radiation resource assessment programs. Within these programs the spatial (geographic) and temporal (hourly, daily, and seasonal) variability of solar radiation at different locations is investigated to reliably predict the energy that will be produced by solar energy systems. In addition to spatial and temporal characteristics, the spectral content of solar radiation is important for designing and predicting the performance of spectrally selective solar energy conversion systems, such as photovoltaic systems. The results of these investigations, however, are applicable to many current research areas, such as daylight availability predictions, radiation models for climate change predictions, and biological impacts of climate change. The discussions presented here pertain to the short-wavelength region of the solar spectrum from the near-ultraviolet (NUV, 300–380 nm) regions through the visible (VIS, 380–780 nm) and near-infrared (NIR, 780–4000 nm) regions.

Except for a few sites worldwide, there have not been and will not be records available on the optical properties of the atmosphere. Thus, a physical model requiring these records as input cannot be used to describe the solar resource at all potential sites for solar energy systems. Therefore, solar radiation resource assessment makes use of semiempirical models, which correlate available meteorological data such as cloud cover, visibility, temperature, humidity, pressure, and some available broadband irradiance measurements to predict irradiance. These semiempirical models are derived from data acquired at a few research stations.

In this study, the solar spectral irradiance was recorded at four different stations, along with meteorological and broadband irradiance, to establish a semiempirical model that can predict solar spectral irradiance at sites where at least the following information is available: hourly records of global and diffuse broadband irradiance, as well as temperature and humidity.

This paper begins with a theoretical discussion on how clouds alter the relative solar spectral distribution (section 2). In section 3, the instrumentation used at the four sites is described and their measurement uncertainty is stated. In section 4, the different datasets are analyzed with two methods to examine how the

Corresponding author address: Dr. Carol Riordan, Solar Energy Research Institute, 1617 Cole Boulevard, Golden, CO 80401.

clouds alter the relative spectral distribution of the solar irradiance measured on the ground. The first method uses a standard spectrum and the second uses a clear-sky simulation for comparison within the measured spectrum. Finally, data from the German site were used to show how to develop a clear- and cloudy-sky semiempirical model using only the four readily available variables mentioned above.

Besides the semiempirical model itself, this report presents the measured variability of the solar spectral irradiance with emphasis on cloudy conditions, which might be useful for improving radiative transfer codes. The datasets are available on disk or tape for further investigation.

2. The shortwave spectral transmission of clouds

Generally, the literature on cloud transmittance suggests that clouds act as somewhat of a neutral density filter in the VIS region of the spectrum. At the upper wavelength limit of the VIS region and in the NIR region, clouds are strong absorbers of radiation in selected wavelength bands. This absorption of radiation by clouds is caused by increased water-vapor absorption at bands centered at 724, 824, 938, 1120, 1400, 1860, and 2700 nm and by liquid-water absorption mostly beyond 1400 nm where the water-vapor absorption bands are not saturated (Love 1988). These absorption effects are difficult to isolate in spectral measurements because there can be a competing enhancement of irradiance resulting from multiple reflections between the clouds and a high-reflectivity ground surface (Nann 1989a). When the ground reflectivity has a strong spectral dependence, such as the high reflectivity of green vegetation in the NIR region as compared to the NUV–VIS region, the cloud enhancement effects on the spectrum also show this spectral dependence.

There is also some evidence, given by radiative transfer codes, that cloud transmittance in the NUV–VIS region of the spectrum is higher for the shorter wavelengths than for the longer wavelengths of this NUV–VIS region because the extinction (scattering and absorption) coefficients and the asymmetry parameter vary with wavelength over this region (Wiscombe et al. 1984; Wiscombe and Welch 1986; Love 1988). Bohren (1990a) concludes that it is the small, nonuniform absorption of visible radiation by cloud droplets which could cause the radiation transmitted by clouds to be bluer than expected. Furthermore, recently reported measurements indicated a relatively higher transmission of 30% and more for the shorter wavelengths than for the longer wavelengths of the NUV–VIS region under cloudy skies (Bird et al. 1987; Paris and Justus 1988; Nann 1990a; Nann and Riordan 1990b).

The net shortwave flux at the surface under an overcast sky is mainly a function of three parameters (Shine 1984): scaled optical thickness τ^*, solar zenith angle z, and surface reflectance $\rho(\lambda)$. Their influence on the relative spectral transmission is described in this section.

a. Cloud optical thickness

Assuming $z = 0$, the transmission T through a uniform cloud layer is related to the scaled optical thickness τ^*:

$$\tau^* = (1 - g)\tau$$

$$\tau = \int_0^h (\kappa + \beta)dh, \tag{1}$$

where g is the asymmetry parameter (mean cosine of scattering angle), κ is the absorption coefficient, β is the scattering coefficient, and h is the cloud thickness.

The transmission T can be treated for a multiple scattering medium like clouds ($\tau^* \gg 1$) with the so-called "two-stream approximation" of radiative transfer, where photons are constrained to be scattered in only two directions, upward and downward. A simplified solution for the radiative transfer equation is given by Bohren (1987). For a nonabsorbing medium ($\kappa = 0$), T is expressed as

$$T = \frac{2}{2 + \tau^*}. \tag{2}$$

Several spectral radiative transfer codes exist, accounting for g, κ, and β to calculate cloud transmission. The droplet-size distribution of the water in the cloud determines the wavelength-dependent scattering parameters g, κ, and β; β increases by about 2%–5% (depending on droplet-size distribution). In the same range, g decreases by 0%–2% (Love 1988). Using typical values for $g = 0.85$, $\beta h = 20$, and $\kappa = 0$ in the UV–VIS region, these variations of β and g can [according to Eqs. (1) and (2)] explain up to a 10% higher transmission for the shorter wavelengths. If $\beta h = 100$ is assumed, then a 5% increase in β, accompanied by a 2% decrease in g, would result in up to an 18% increase in T for the shorter wavelengths. The variability with drop distribution, while seemingly small, can be significant because in radiative transfer it is not g itself, but $(1 - g)$, which becomes important.

Bohren (1990, personal communication) points out that the Wiscombe et al. (1984) paper shows calculated extinction coefficient (i.e., scattering) and the asymmetry parameter varying by only about 1% over the visible region; and, the only parameter that varies appreciably (300%–400%) over the visible region is the absorption coefficient k. Therefore, if light transmitted by clouds is bluish and measurements show 30% higher transmission or more for the shorter wavelengths, it must be the result of preferential absorption by cloud droplets (according to our rough calculation applying eqs. 1 and 2 with $k = 0$).

The most pronounced spectral effects are at wavelengths where the clouds absorb the incoming radiation

in selected wavelength bands. At 724, 824, 938, and 1120 nm absorption by water vapor molecules in a cloud or a cloudy atmosphere is the dominant process (Love 1988). Water-vapor absorption is sharply peaked at the absorption wavelengths and becomes quite small in intervening wavelength regions. Absorption by liquid water becomes the dominant process at 1400, 1860, and 2700 nm. The peaks are less marked with absorption extending over a broader wavelength region. For a thick cloud ($\tau > 50$), there is almost no radiation reaching the surface beyond 1860 nm (see Fig. 1 and Welch et al. 1980).

b. Solar zenith angle

The cloud optical thickness τ^* is defined in a vertical path. Therefore, the "effective" cloud optical thickness increases with the solar zenith angle z, and the transmission T becomes a function of both τ^* and z. As cloud thickness increases, however, the original direction of the incoming beam is lost due to multiple scattering events.

c. Surface reflectivity

The reflectivity of the cloud in the VIS region is very high (up to 70%) compared with the atmospheric albedo of a clear sky (around 10% at 500 nm). Therefore, multiple reflection between the ground surface and clouds becomes important, especially for a highly reflective surface (Middleton 1954). Under an overcast sky with a cloud-base height of approximately 1 km, radiation reflected from an area of approximately 4-km diameter (assuming a maximum reflection angle of 45°) is seen by a horizontally oriented detector. Site-specific measurements are influenced by mixed albedos composed of several natural and developed surfaces of the site. Furthermore, the albedo is seasonally dependent because of phenomena such as vegetation cycles and snow cover (Brest 1987). Detailed albedo information can only be obtained by image segmentation (texture analysis) of satellite images or aerial photos of the given site.

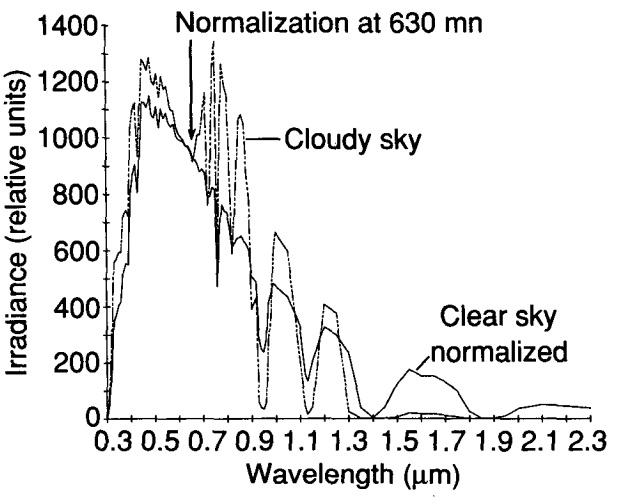

FIG. 1. Simulated spectra under clear-sky ($\tau = 0$) and overcast-sky ($\tau = 128$) conditions, normalized at 630 nm. The calculations were performed using the Paris/Justus code.

The effect of multiple reflection between a cloud and the ground is demonstrated by a two-stream approximation code (Paris 1985). The three parameters characterizing the homogeneous cloud layer are cloud optical thickness τ, asymmetry factor g, and the absorption coefficient κ. A wavelength-dependent form of these parameters for a (typical) cumulus cloud-droplet-size distribution is assumed in this radiative transfer code. Figure 1 compares the shape of the calculated global horizontal spectra for $\tau = 0$ (no clouds) and $\tau = 128$ (a very thick cloud layer). Both simulations were performed with the same inputs (except for τ): 1.42 cm precipitable water vapor, aerosol optical depth of 0.27 at 500 nm, and a spectral ground reflectance representing green vegetation that is generally low (0.1) in the VIS region and relatively high (0.6) in the NIR region. The spectrum for $\tau = 128$ was normalized to the clear-sky spectrum by multiplying the cloudy spectrum by the ratio of clear to cloudy irradiance at 630 nm, which is 12.1 for this example. The simulations show a peak in spectral irradiance beyond the chlorophyll absorption band at 650 nm from the high reflectance of green vegetation. Figure 1 also predicts (according to the previous discussion) other deviations from a spectrally constant cloud transmittance function. That is, the spectrum under an overcast sky has a higher transmission in the UV and blue (300–500 nm) regions relative to the normalization point at 630 nm. Also, water-vapor and droplet absorption are more pronounced in the NIR region for the cloudy-sky simulation.

3. Solar spectral irradiance measurements in Germany and the United States

Both ZSW and SERI used similar instrumentation and similar strategies in data acquisition. Because the majority of data analyzed in this report were taken at the German site, the ZSW data acquisition system is described in more detail; the major differences in the United States data acquisition system are pointed out later.

a. The German dataset (ZSW)

The ZSW solar spectral irradiance data acquisition station SEDES (see Fig. 2) was designed for permanent and remote outdoor operation in a humid and cloudy climate with low sun elevations. It recorded about 12 000 spectra between July and November 1989. The station is located at Stuttgart (49°N, 9°E). A spectral scan is recorded every 5 min, but only when the broadband irradiance did not change by more than ±5% within the 12-s scan time. Six scans are averaged and stored on disk. Thus, the database consists of about

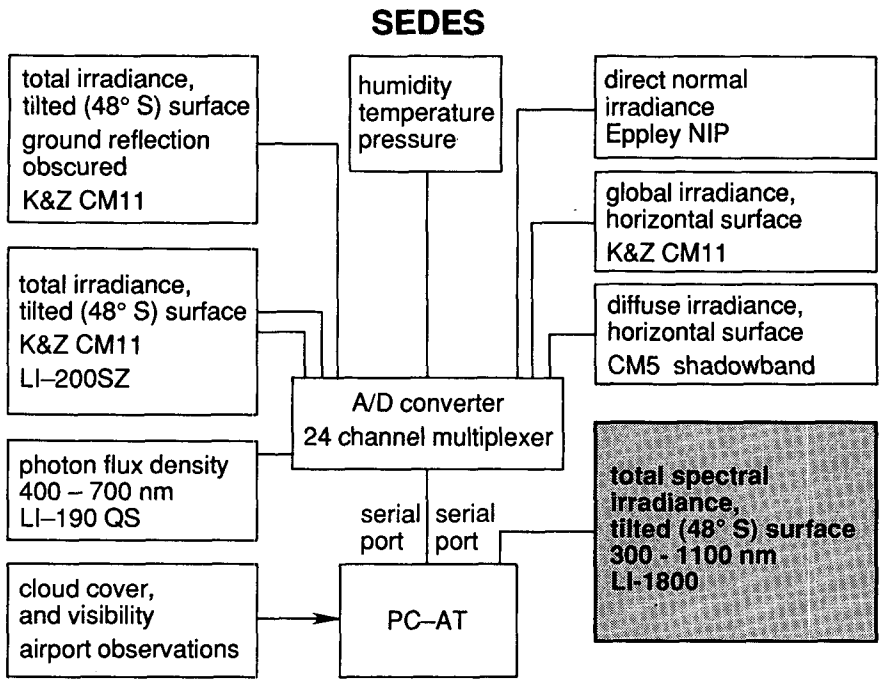

FIG. 2. The different instruments of the solar spectral irradiance data acquisition station SEDES at Stuttgart.

2000 half-hourly measurements of the spectral irradiance on a 48° tilted plane. SEDES simultaneously records several broadband irradiance values and also humidity, temperature, and pressure. The nearby (10 km) airport provides total cloud cover and visibility observations. The station is located 70 m above ground on the top of a building within a university campus. Approximately half the surrounding surface is covered by forest. All instruments were calibrated before and after the measurement period, and the station was visited three times a week or more to check instruments.

1) ABSOLUTE MEASUREMENT UNCERTAINTY OF THE SPECTRORADIOMETER

The spectral measurements were performed with a LI-COR model LI-1800 spectroradiometer with a Teflon dome diffuser and holographic grating monochromator using a 10-nm step size (6-nm bandpass) between 300 nm and 1100 nm. The whole device is air conditioned in a case to allow long-term exposure and reduce changes in calibration caused by temperature response. SERI and ZSW extensively investigated the

TABLE 1. Absolute measurement uncertainty for direct normal irradiance (%).

Wavelength range (nm)	B_c	B_d	B_t	σ_1	σ_{10}	U_{66}	U_{95}
320–350	5	5–3	—	12–3	4–1	15–7	26–9
350–400	4	3–1	—	3–0	1–0	6–4	8–4
400–1000	4	—	—	0	0	4	4
1000–1100	5	—	0–2	0	0	5–6	5–6

B_c = bias error from calibration accuracy (manufacturer).
B_d = bias error from degradation between calibrations (estimated).
B_t = bias error from temperature drift after the temperature correction is applied (measured).
$B = (B_c^2 + B_d^2 + B_t^2)^{0.5}$.
σ_{10} = random error of the calibration file (recorded from the mean of ten subsequent measurements).
σ_1 = random error of a single measurement (calculated from σ_{10}).
$\sigma = (\sigma_1^2 + \sigma_{10}^2)^{0.5}$.
$U_{95} = [B^2 + (2\sigma)^2]^{0.5}$: absolute ($2\sigma$) measurement uncertainty.
$U_{66} = (B^2 + \sigma^2)^{0.5}$: absolute ($1\sigma$) measurement uncertainty.

absolute measurement uncertainty of this spectroradiometer (Myers 1989; Nann 1989b). The ZSW instrument, calibrated with a 200-W tungsten halogen lamp, has an outdoor measurement uncertainty (for a normal incidence direct solar beam) of 4% between 400 and 1000 nm (see Table 1). In this wavelength range, the absolute measurement uncertainty is dominated by the calibration accuracy of the lamp and the calibration process itself. The reference lamp of SERI was measured with the instrument being calibrated at ZSW. This lamp is calibrated by the U.S. National Institute for Standards and Technology (NIST) and has a lower uncertainty than the ZSW lamp calibrated by LI-COR. The comparison confirmed the 4% uncertainty between 400 and 1000 nm and, in addition, established the transferability of solar irradiance measurements between the two laboratories.

Beyond 950 nm, the temperature sensitivity of the spectroradiometer increases the absolute measurement uncertainty. A temperature sensor attached to the detector records any deviation from the calibration temperature. The spectroradiometer readings were corrected between 950 and 1100 nm by the known temperature response of the detector (Myers 1989). Because of the air conditioning, these deviations were only within a few degrees Celsius. Therefore, the absolute measurement uncertainty of the device beyond 1000 nm is again mainly dominated by the calibration accuracy of 5% between 1000 and 1100 nm.

Below 400 nm, three more sources increase the absolute measurement uncertainty: random error during calibration, random measurement error, and degradation of the optical entrance. The latter depends very much on the age of the Teflon dome diffuser and the calibration frequency, and was about 5% at 320 nm for a three-month exposure based on estimates from the calibration files. The random errors are mainly caused by electrical noise and stray light. The calibration lamp intensity below 400 nm is very low, but the irradiance received from the lamp between 320 and 400 nm matches the irradiance received on a dark, overcast day. Thus, a "worst case estimate" was obtained for the device's random measurement uncertainty (on an overcast day) from repeated measurements of the calibration source. The random measurement error of one scan determined from ten measurements of the lamp was found to be 12% at 320 nm and almost 0% at 400 nm. Because the calibration file itself is taken from ten measurements, the random component of the calibration accuracy is reduced by a factor of $10^{-1/2}$.

For the measurements being reported here 13 July–27 November 1989) and the calibration performed at Stuttgart before and after this period (as well as at SERI after this period), we estimate the absolute measurement uncertainty U_{95} of one scan (for a normal incidence direct beam) according to Table 1.

The instrument is calibrated with a collimated beam. The distribution of the skylight, however, covers the 2π field of view of the spectroradiometer's optical entrance. Moreover, the incidence angle of the sun's direct beam covers the whole range from 0° to 90°. The cosine response of the Teflon dome diffuser was investigated through laboratory tests at SERI and ZSW for incidence angles between 0° and ±75° for all four principal azimuth orientations of the device. For almost all wavelengths and angles of incidence, the cosine response turned out to be less than expected from Lambert's law. This is mainly for higher wavelengths where the Teflon material becomes excessively transparent. Figure 3 shows the result of the worst case azimuthal orientation. The cosine error at 1100 nm and an incident angle of 75° is −45%. It should be noted, however, that LI-COR now offers another Teflon material that reduces the cosine errors, according to the measurements, by a factor of two. Furthermore, the error decreases up to a factor of two for other azimuthal orientations. The error due to imperfect cosine response is reduced because the spectroradiometer is tilted at 48° south, which reduces the angle of incidence of the direct beam throughout most of the day as compared to a horizontal orientation.

Based on this uncertainty analysis, the data analysis is restricted to angles of incidence less than 72° and to a wavelength range from 320 to 1050 nm. Because of the cosine error, however, the measurements for angles of incidence greater than 60° with a direct solar beam present have a significant bias error. On the other hand, up to 950 nm the cosine response is wavelength independent. Under overcast skies with an istropically distributed radiance, the shape of the measured spectrum is not affected by the cosine response of the Teflon dome.

2) Data selection

The 2000 half-hourly records were checked with first-order methods to ensure data quality. A dataset was

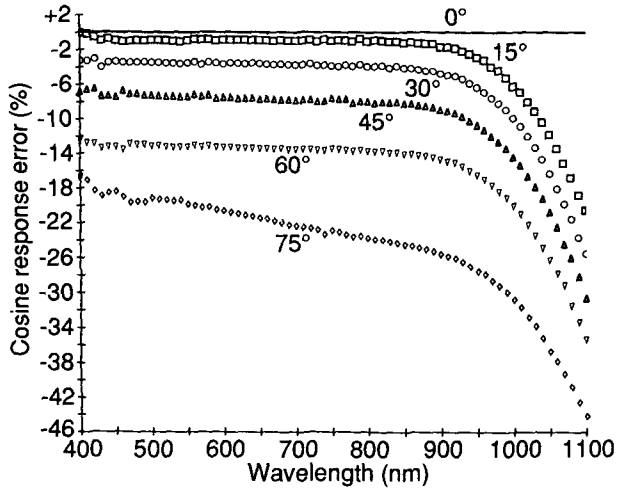

FIG. 3. Cosine response of the LI-COR 1800 equipped with a Teflon dome diffuser (original Teflon dome, worst azimuthal orientation).

eliminated if the following conditions were not met: visibility (meteorological range) $\geq$ 4 km; solar elevation $> 10°$ (relative air mass < 6); global and total tilted pyranometer readings > 40 W m^{-2} (half-hourly average) and 80% of the maximum possible (extraterrestrial irradiance projected onto the given surface); diffuse irradiance [after shadow-band correction applied (Kasten et al. 1983)] between 0.075 and 1.075 of global irradiance and less than 0.5 of the extraterrestrial irradiance on a horizontal surface. In addition, the calibration stability (traceable to the World Radiation Center) of all pyranometers was monitored by comparing the long-term ratio of the different devices (see Fig. 2) that did not change by more than 3%. The reference pyranometer at the German site was calibrated at SERI after the measurement period. The agreement of the calibration factors was excellent. The spectroradiometer data were checked for a minimum of five scans in each 30-min segment that passed the 5% stability check. The average number of scans for each half hour is 5.9; that is, 90% consist of six scans and 10% consist of five scans.

The combination of these data selection measures eliminated mainly the records close to sunrise and sunset, during foggy conditions, and situations with high reflections from the ground or clouds. After all data selection criteria were applied, 1038 half-hourly measurements were left.

An overcast sky was defined by total cloud cover (hourly records) of 7 or 8 octa and by a ratio of diffuse to global horizontal irradiance (K) greater than 0.90. Actually, the mean of K for the overcast dataset is 0.98. A clear sky was defined by total cloud cover of 0 or 1 octa and by a ratio of global-horizontal to extraterrestrial irradiance [clearness index K_t, see Eq. (6)] greater than 0.6. [This may have eliminated cases with low solar elevations because K_t decreases with the zenith angle for a given sky condition (Perez et al. 1990b).] The mean of K_t for the clear-sky dataset is 0.68. This clear-sky dataset still can contain some cirrus clouds. Table 2 gives more variables characterizing the dataset that will be analyzed in section 4.

Estimates for water vapor and aerosol optical depth at 500 nm for the German dataset are also given in Table 2. These two variables, together with geometry, are the most important parameters for determining solar spectral irradiance for a cloudless atmosphere. We used the information available from the meteorological data, which were recorded simultaneously with the spectral measurements, and approximation formulas discussed hereafter to calculate these two values.

Recently, Garrison and Adler (1990) proposed a relationship between monthly precipitable water W (cm) and monthly mean surface temperature T (K), along with relative humidity Φ (%) for 82 sites in the contiguous United States and Alaska:

$$W = \frac{0.41173\Phi P}{1013T} e_s + 0.2, \tag{3}$$

where P is the surface pressure (mb) and e_s is the saturated vapor pressure of water (mb)—a function of the absolute temperature. This regression equation, founded on experimental results, gives water vapor amounts similar to an equation formulated by Leckner (1978), which was based solely on theoretical assumptions. Similar relationships were found by others (Reitan 1963; Bolsegna 1965; Smith 1966; Tomasi 1981).

TABLE 2. Characteristics of the ZSW dataset (based on half-hour averages).

	Global irradiance (W m^{-2})	Diffuse irradiance (W m^{-2})	Aerosol optical depth (at 500 nm)	Precipitable water (cm)	300–1100 nm[a] / 300–4000 nm (%)	Zenith angle (deg)	Angle of[b] incidence (deg)	Cloud cover (octa)
				Whole data set[c] (1038 records)				
Max	898	481	0.82	3.17	100	80	72	8
Mean	322	157	0.23	1.73	78	58	37	4.8
Min	47	27	0.04	0.54	60	28	4	0
				Overcast sky (331 records)				
Max	532	479	0.82	3.14	100	80	72	8
Mean	144	140	0.30	1.83	82	59	36	7.4
Min	47	47	0.04	0.96	61	28	4	7
				Clear sky (161 records)				
Max	875	335	0.73	2.38	86	78	72	1
Mean	468	102	0.19	1.46	75	59	34	0.61
Min	172	29	0.04	0.54	69	29	4	0
AM 1.5 standard spectrum[d]:			0.27	1.42	80	48	11	0

[a] Integrated spectroradiometer reading divided by the pyranometer reading.
[b] Angle between the instrument's axis and the sun's position.
[c] The whole dataset is composed of overcast, clear sky, and partly cloudy conditions.
[d] See section 4.

An investigation using dewpoint and water-vapor measurements at Albany, New York, even found a correlation for instantaneous values (Wright et al. 1989). Therefore, Eq. (3) was applied to calculate the precipitable water vapor for the half-hourly data, although the relationship has mainly been proven for monthly averages.

After Koschmieder's (1924) basic investigations, several experiments proved a moderate correlation between the horizontal meteorological range V (visibility in kilometers, km) and the vertical turbidity (aerosol optical depth) t for a cloudless atmosphere (Eltermann 1970; McClatchey and Selby 1972; Kriebel 1978; Peterson and Fee 1981):

$$t(550\text{ nm}) = H\left(\frac{3.0}{V} - 0.0146\right). \quad (4)$$

The value 3.0 instead of 3.9 is used for a contrast threshold of 0.05, which is normally applied for the German network observations available in the database (Kasten personal communication). The small coefficient of 0.0146 corrects for Rayleigh scattering and ozone absorption at 550 nm in the horizontal path. The quantity H, the aerosol scale height, gives the vertical extent of the homogeneous haze layer in which the aerosol extinction coefficient is assumed to be constant with altitude.

However, H depends on the actual state of the atmosphere and the site. Using broadband measurements of direct normal irradiance and the pyrheliometric formula (Kasten 1980), we found an aerosol scale height of $H = 2.5$ km on a clear day in September and $H = 0.4$ km on a cold clear winter day. Tomasi (1982) found similar results for cold atmospheres with inversion layers ($0.5 < H < 1.3$ km) and summer days with strong convective motions ($H > 2$ km). According to Volz (1969), an average value $H = 1.25$ km can be applied for the site. The measurement station SEDES, however, is located at a higher elevation than the airport. Therefore, a somewhat lower mean value (1.0 km) was chosen for H. The uncertainty of visibility observation itself (about ±10%) becomes minor in view of the huge uncertainty in H.

Finally, the relationship between the meteorological range V and the turbidity (aerosol optical depth) t was derived from measurements with a direct beam present. Currently, there is no information about how these two quantities are correlated under cloudy skies. Therefore, our knowledge of aerosol optical depth is very uncertain. Moreover, there is no information at all on the particle-size distribution, which determines α in the Angström formula. Although Eq. (4) was applied to estimate the aerosol optical depth at 500 nm for the whole dataset (using $\alpha = 1.14$ as wavelength exponent to translate from 550 to 500 nm).

b. The United States dataset (SERI)

An independent database from SERI (Riordan et al. 1989) consists of data acquired at the Florida Solar Energy Center at Cape Canaveral, Florida, and Pacific Gas and Electric Company in San Ramon, California, over about a 1-year period and by SERI in Denver and Golden, Colorado, during one-winter season. This database consists of individual spectral irradiance scans measured with a LI-COR model LI-1800 spectroradiometer (modified with an integrating sphere and temperature controller) from 300 nm to 1100 nm with a 6-nm bandpass and 2-nm steps. An irradiance stability monitor was operating when the scans were acquired so that no scans were recorded if the total irradiance varied by more than ±2% within the 30-s scan time. The spectroradiometer was calibrated and operated at 40°C. Meteorological and broadband data, such as global-horizontal irradiance, were recorded before and after each scan. The absolute measurement uncertainty is similar to that of the ZSW instrument (see Table 1).

In comparison with the ZSW data, the SERI data are individual spectra (rather than half-hourly averaged spectra) acquired at 2-nm steps (rather than 10-nm steps). The longer scan time, along with a more restrictive irradiance stability criteria (2% rather than 5%), mean that the SERI dataset contains a fewer percentage of records under cloudy conditions. Also, an integrating sphere (rather than a Teflon diffuser) was used as the receiver on the LI-COR spectroradiometer.

To avoid considerations of ground reflected irradiance onto the spectroradiometer, only global-horizontal spectra were selected from the database for analysis. (The German dataset consists of measurements made with the spectroradiometer tilted 48° from the horizontal.) However, multiple reflections between the ground and the sky or cloud are still a consideration. The global-horizontal dataset contained 356 spectra from Cape Canaveral, Florida; 56 from San Ramon, California; and 31 from Denver and Golden, Colorado. The Florida location is relatively humid compared to the California and Colorado sites, which are relatively dry. Records were selected with zenith angles less than 76°, with K_t values from 10% to 90%, and with a maximum ratio of direct-to-global horizontal irradiance of 90%. Characteristics of the SERI set (all sites) are given in Table 3.

4. The influence of clouds on the relative spectral distribution of solar irradiance at the ground

The ZSW and SERI datasets were first analyzed by the two research groups independently. The common question raised was how the spectral transmission of clouds deviates from an assumed neutral density filter. The common approach was to compare the measured spectrum with the spectrum of a clear-sky reference spectrum after the reference spectrum had been normalized by the ratio of measured and reference spectrum at 630 nm (Nann and Riordan 1990b):

TABLE 3. Characteristics of the SERI dataset (based on individual spectra) [whole dataset (443 records)].

	Global irradiance (W m^{-2})	Clearness index K_t	Precipitable[a] water (cm)	Zenith angle (deg)
Max	1143	0.89	12.4	76
Mean	629	0.67	3.8	44
Min	37	0.11	0.2	5

[a] See section 4b.

$$R(\lambda) = \frac{\text{measurement}(\lambda)}{\text{reference}(\lambda)} \frac{\text{reference}(630\text{ nm})}{\text{measurement}(630\text{ nm})}. \quad (5)$$

If clouds act as a neutral density filter, the resulting ratio $R(\lambda)$ should be 1.0 for the wavelength range investigated. The normalization at 630 nm is necessary to account for the different bulk atmospheric transmission for measured and reference spectrum. At 630 nm, water-vapor and droplet absorption do not affect the transmission (except for the minor visible absorption of liquid water as described in section 2). Second, scattering caused by air molecules and aerosols is less important than at shorter wavelengths.

a. *Comparison of the German dataset with the ASTM standard*

The American Society for Testing and Materials (ASTM) and others have adopted particular spectral irradiance datasets as standard reference spectra. One of these is the "standard for solar spectral irradiance tables at air mass 1.5 for a 37° tilted surface" (ASTM Standard E892-87). A possible approach to analyzing the measured spectra is to compare them with the shape of this standard spectrum. The standard air mass (AM) 1.5 (zenith angle of 48.2°) spectrum calculated with the BRITE code (Hulstrom et al. 1985) was first transformed to the 10-nm step size of the spectroradiometer. Next the ratio $R(\lambda)$ was derived according to Eq. (5).

The mean of all ratios $R(\lambda)$ with standard deviation $\sigma(\lambda)$ is plotted in Fig. 4a for all wavelengths. Between 350 and 900 nm, the mean of $R(\lambda)$ lies within 1.0 and 1.1, which means that the ASTM standard is a reasonable representation for the shape of the measured average spectrum. There are, however, some systematic deviations for the UV–blue region, the region beyond the chlorophyll absorption band at 650 nm (from albedo effect), and the strong water-vapor absorption band around 940 nm. Figure 4b, which shows the ratio $R(\lambda)$ for the overcast data only, allows the hypothesis that the systematic deviations mainly occur under overcast-sky conditions. Figure 4c shows $R(\lambda)$ for the clear-sky data sample and supports this hypothesis, also, because the deviations are less or are even in the opposite direction (in the UV) compared to the overcast case. We tried several other hypotheses, such as whether the deviations are correlated with aerosol optical depth, water vapor, cosine of the zenith angle (air mass), cosine of the angle of incidence (cosine error of the instrument), and day of the year. There is a dependence of $R(\lambda)$ on the zenith angle for the clear-sky data sample and a dependence on the day of the

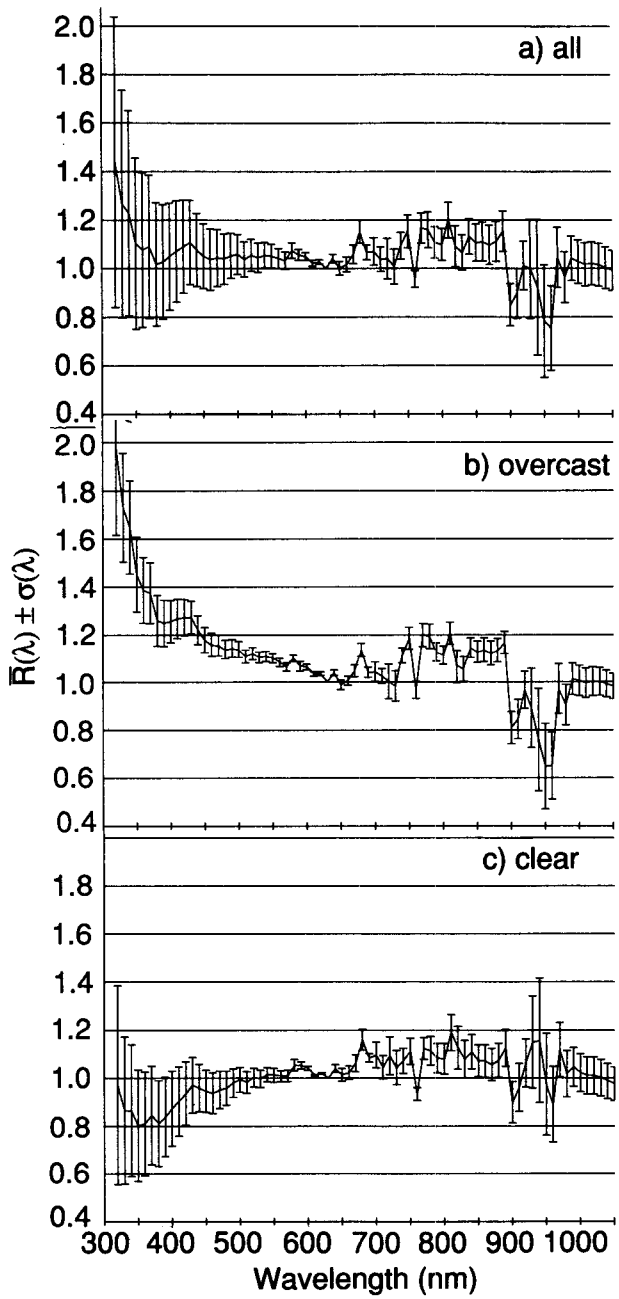

FIG. 4. The complete German dataset of spectral measurements (a) along with only overcast-sky (b) and clear-sky (c) measurements, all divided by the ASTM standard spectrum. Shown is the mean of $R(\lambda)$ and $\pm\sigma(\lambda)$ for each wavelength derived from Eq. (5) (normalization at 630 nm).

year, especially for the overcast-sky sample, which will be discussed later.

To establish a relationship between these spectral effects and clouds, the spectral shift was examined as a function of atmospheric (cloudy sky) transmittance using a clearness index K_t:

$$K_t = \frac{I}{I_o \cos z}, \tag{6}$$

where I is the global (broadband) irradiance on a horizontal surface and $I_o \cos z$ is the extraterrestrial irradiance on a horizontal surface with z as zenith angle. The clearness index K_t was applied as a measure for the cloud optical thickness τ. As long as the dataset consists solely of total overcast-sky samples, K_t is correlated mainly with the cloud optical thickness (Paris 1985; Shine 1984), although K_t is also influenced by zenith angle, aerosols, and water vapor. We performed a least-squares fit of the (intrinsically linear) functional form

$$R(\lambda, K_t) = \exp[A(\lambda) + B(\lambda)K_t] \tag{7}$$

to the overcast dataset using K_t as the independent variable. Also used were more sophisticated clearness or cloud parameters that were corrected for the zenith dependence (Perez et al. 1990b), but the correlation coefficient between $R(\lambda)$ and these other independent variables increased only slightly. Figure 5 gives the coefficients $A(\lambda)$ and $B(\lambda)$ along with the standard deviation of the regression.

The strength of the correlation between K_t and $R(\lambda)$ can be seen in Fig. 6. The correlation coefficient $|r|$ measures the degree of linear relationship among variables (r^2 gives the percentage of variation explained by

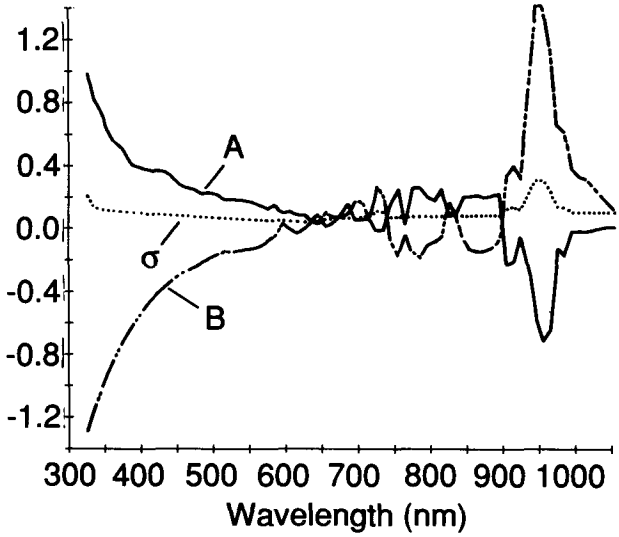

FIG. 5. Coefficients $A(\lambda)$ and $B(\lambda)$ of Eq. (7) for overcast-sky conditions and the standard deviation of the regression. Using $A(\lambda)$ and $B(\lambda)$, one can estimate the relative spectral distribution under an overcast sky from the ASTM standard for the German site.

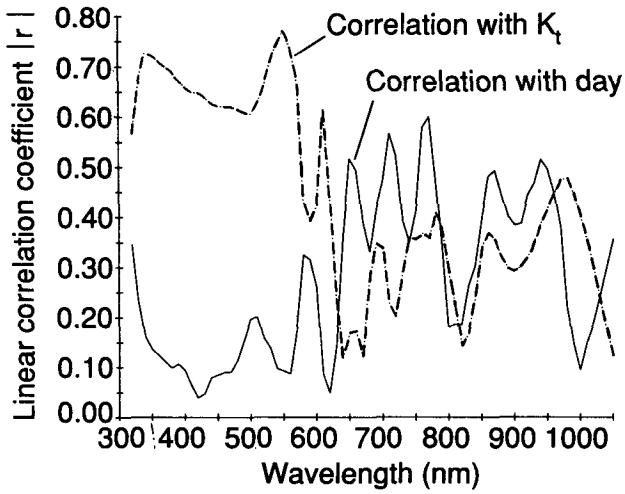

FIG. 6. Correlation coefficients $|r(\lambda)|$ of Eqs. (7) and (8) for an overcast sky of the German dataset.

the regression). To smooth the high fluctuations in $|r(\lambda)|$ because of the different wavelength resolutions between measurement and model, this plot was averaged over three 10-nm bins each. The results show that K_t is strongly correlated with the higher transmission under clouds (relative to the standard) in the UV and blue regions, and weakly correlated with the albedo enhancement beyond the chlorophyll absorption band. The correlation for the water-vapor band around 940 nm is not surprising because the water vapor amount for the standard spectrum is less than calculated for the overcast-sky sample (see Table 2).

The linear correlation coefficient $|r|$ of Fig. 6 with the day number (DAY) as the independent variable was calculated from

$$R(\lambda, DAY) = C + D[183 - \text{abs}(DAY - 183)]. \tag{8}$$

The albedo enhancement (see section 2) is moderately correlated with the day number. The albedo enhancement becomes weaker throughout the second half of 1989, as the vegetation changes color from green to brown. Not only is the "albedo effect" seasonally dependent, but so also are the general climatological conditions, including the physical constitution of the clouds. Even at the water-vapor absorption band at 940 nm, there is a seasonal trend for the relative spectral distribution. There is a weak correlation with the day number for wavelengths below 600 nm. This correlation is for zenith angles greater than 65° on clear days (see Fig. 4c). These high zenith angles occur mainly in November and December; therefore, there is a correlation with day number.

b. Comparison of the United States dataset with the ASTM standard and a clear-sky simulation

The ASTM standard was again applied as a reference spectrum to analyze the measurements of the United

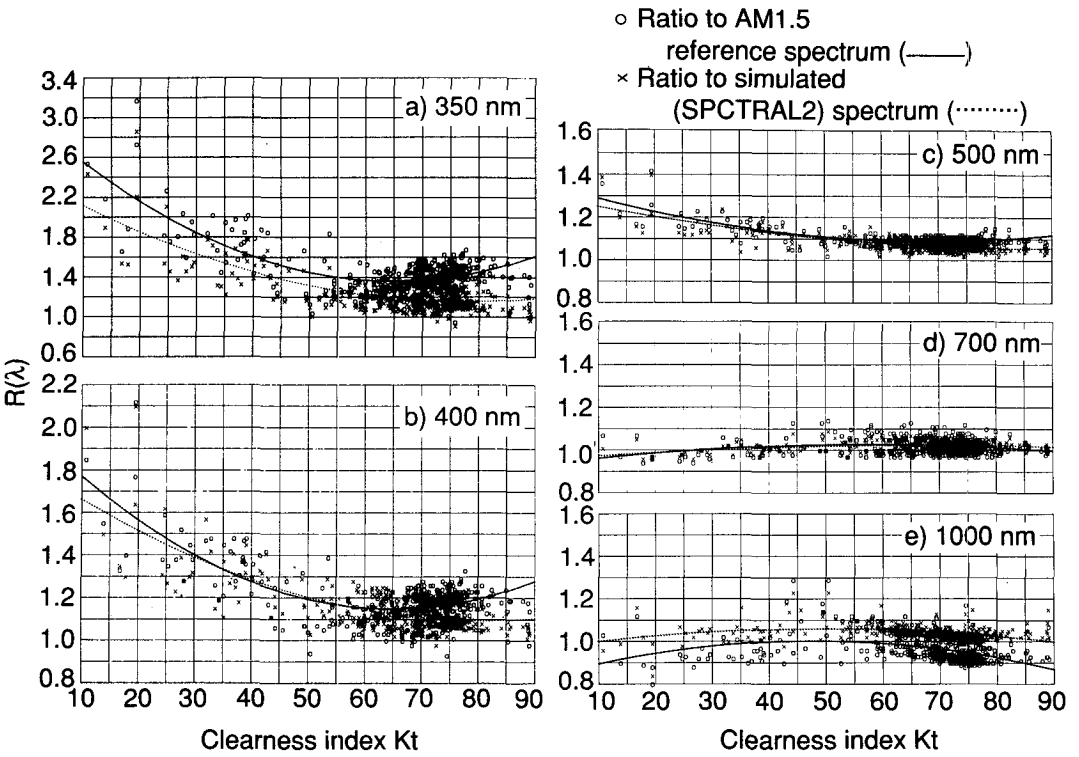

FIG. 7(a)–(e) The complete United States dataset of spectral measurements divided by the normalized clear-sky simulation and the ASTM standard spectrum. Shown is $R(\lambda)$ derived from Eq. (5) (normalization at 630 nm).

States dataset after being linearly interpolated to the 401 measured wavelengths (2-nm resolution) and normalized to 630 nm. Ratios of measured to normalized values were then calculated according to Eq. (5) and are plotted as a function of the clearness index in Fig. 7 for the entire United States dataset. Both the measured and the reference spectra were smoothed (moving the average over 20 nm) to reduce small wavelength or resolution differences in rapidly changing regions of the spectrum (e.g., near the oxygen absorption band at 762 nm).

A second way to analyze the measured relative spectral distribution is to compare it with the corresponding clear-sky simulation (i.e., if no clouds had been present). The SPCTRAL2 model (Bird and Riordan 1986) was applied using as input an aerosol optical depth (at 500 nm) of 0.1 and a ground reflectance of 0.2 besides solar geometry. In an iterative routine the precipitable water vapor was derived by matching the depth of the absorption band in the simulated spectrum to the measured spectrum at 938 nm. The high range of calculated water vapor (see Table 3) is caused by including both humid (Florida) and dry (California and Colorado) sites in the United States dataset. Again after interpolating and smoothing the spectra, the ratios $R(\lambda)$ according to Eq. (5) were calculated.

Figures 7a–e show the ratios of measured to normalized, reference spectra (SPCTRAL2 simulations and the AM 1.5 standard spectrum) as a function of K_t at selected wavelengths for the entire United States dataset. (Cases where K_t values were less than 40% were identified as cloudy skies because direct irradiance was less than 10%.) These plots show a distinctly higher relative transmittance of UV and blue irradiance under cloudy skies.

Figure 8 shows examples of the ratios of measured to normalized SPCTRAL2 simulations for all wavelengths for a few typical cloudy- and clear-sky cases.

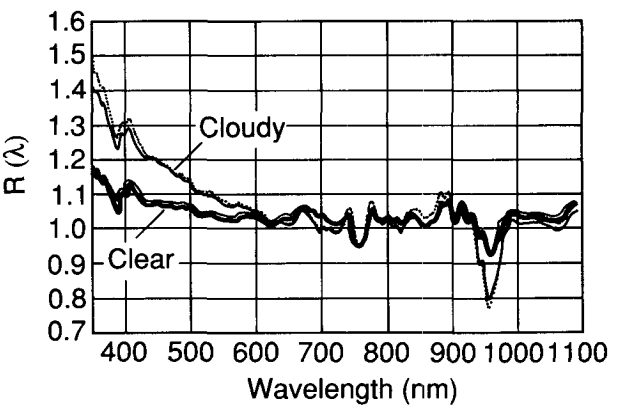

FIG. 8. Typical ratios $R(\lambda)$ of measured to simulated (clear sky) spectra for cloudy- and clear-sky cases of the United States dataset derived from Eq. (5) (normalization at 630 nm).

Both the cloudy and clear cases show higher ratios in the UV and blue regions with the cloudy cases showing a larger difference.

High-frequency deviations from 1.0 are mostly caused by resolution differences between measured and modeled spectra near absorption bands.

For all cloudy-sky cases in the dataset ($K_t < 40\%$), the ratio of integrated irradiance between 300 and 400 nm to total irradiance (300–4000 nm) averages 6.8%, whereas it averages 6.1% for clear-sky cases ($K_t > 60\%$). The ratios of 400–700 nm to total irradiance are 52% and 46% for cloudy- and clear-sky cases, respectively. The ratios of 300–1100 nm to total irradiance are 93% and 83%, respectively.

c. *Results of the data analysis*

From the analysis of the German and United States datasets (1481 spectra from four sites), the following may be concluded:

- Clouds alter the shape of the spectrum, especially in the UV and blue regions; this effect is correlated with the clearness index K_t, a measure for the cloud optical thickness.
- If there is a seasonal variation in the surface cover, the correlation can be improved by binning the data into different seasons.
- The SPCTRAL2 simulations match the relative spectral distribution very well for clear skies. However, the results show that about a 10% correction is required for wavelengths below 400 nm.
- The ASTM standard represents the relative spectral distribution within ±10% under clear skies except for in the UV and water-vapor region. The deviations for the shorter wavelengths increase with increasing zenith angle.

It should be noted that the entire analysis was restricted to zenith angles less than 80°. The results also have to be compared with the spectroradiometer's measurement uncertainty. However, the absolute uncertainty as stated in Table 1 has been reduced by the normalization procedure; thus, the bias errors become relative to 630 nm. The reason why this study used two different reference spectra (the ASTM standard and the SPCTRAL2 simulation) was to avoid systematic errors that could be caused by applying an incorrect clear-sky model only. The results from this data analysis were applied to develop the semiempirical spectral model for clear and cloudy skies presented in the following section.

5. A semiempirical model for clear and cloudy skies

The analysis in section 4 showed that a semiempirical model for predicting global solar spectral irradiance under clear and cloudy skies can make use of the SPCTRAL2 code in combination with a regression model like proposed in Eq. (7). A general semiempirical model, however, must make use of another normalization method rather than the spectroradiometer signal at 630 nm. Furthermore, this model should work for partly cloudy sky conditions (neither overcast nor clear) that have not yet been discussed. The situation is very complicated under partly cloudy skies. In the partly cloudy case, each component of direct and diffuse radiation (such as clear- and cloudy-sky ratios and reflected radiation) must be weighted. Depending on cloud cover and geometry, solar zenith, and collector orientation, clouds modulate the spectral irradiance by varying the mixture of the different components of radiation.

In practice, the uncertainties in the actual states of the atmosphere, including optical and geometric characteristics of clouds, are more significant than differences in theoretical accuracy. Complex input data are not available to verify sophisticated radiation transfer codes dealing with broken clouds (Welch et al. 1980; Powell 1986) and will certainly not be available on a routine basis. Therefore, the approach proposed here is based on commonly acquired meteorological and broadband solar radiation data only: pressure, temperature, relative humidity (or dewpoint temperature), and global and diffuse (or direct) broadband irradiance. Currently, global and diffuse irradiance constitute the most widely available type of irradiance data. This model, which will be called SEDES1, consists of three parts (see Fig. 9):

(i) Calculate a clear-sky spectrum incident on a horizontal surface (if no clouds were present) using

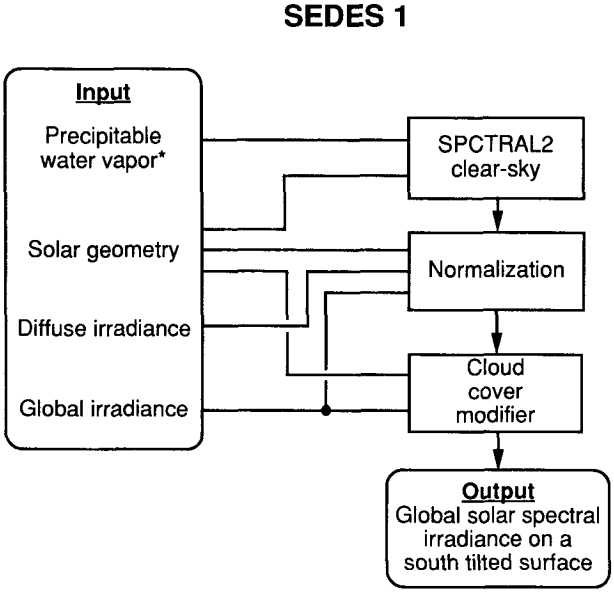

FIG. 9. The principal components of the semiempirical spectral model.

SPCTRAL2 (Bird and Riordan 1986) and Eq. (3) to estimate precipitable water vapor.

(ii) Normalize the simulated clear-sky direct and diffuse irradiances to the measured broadband global and diffuse irradiances using Eq. (9).

(iii) Apply a correction function CCM (λ, K_t), which may be seasonally and site dependent.

In the following, only the data from the German site are analyzed because the United States dataset lacks sufficient data with K_t values less than 0.6 to establish a stable correlation for cloudy skies. The aerosol optical depth at 500 nm (an input for SPCTRAL2) is set to an average value of 0.23, which was calculated from the visibility data of the German site using Eq. (4). Using the actual visibility information available improves the results only slightly.

a. Normalization method

The normalization method accounts for the overall bulk atmospheric transmission. It transforms the components of the clear-sky spectrum to any south-tilted surface, assuming the clouds act as a wavelength-independent filter on the clear-sky spectrum:

$$E'_\alpha(\lambda) = \{[E_b(\lambda)\cos z + E_d(\lambda)]NGH - E_b(\lambda)\cos z NDIR\}\frac{I_{d\alpha}}{I_d} + E_b(\lambda)\cos\alpha NDIR$$

$$NGH = \frac{I}{\int_{300\text{ nm}}^{4000\text{ nm}} [E_b(\lambda)\cos z + E_d(\lambda)]d\lambda}$$

$$NDIR = \frac{I - I_d}{\int_{300\text{ nm}}^{4000\text{ nm}} E_b(\lambda)\cos z d\lambda} \qquad (9)$$

where

$E'_\alpha(\lambda)$ = normalized spectral irradiance on a tilted surface (tilt angle α)
$E_b(\lambda)$ = calculated clear-sky direct normal irradiance (beam irradiance)
$E_d(\lambda)$ = calculated clear-sky diffuse irradiance
I = measured global-horizontal broadband irradiance
I_d = measured diffuse-horizontal broadband irradiance
$I_{d\alpha}$ = measured or calculated diffuse broadband irradiance on a tilted surface (tilt angle α).

Besides the clear-sky model, the normalization method uses only I and I_d (or, alternatively, beam irradiance I_b if available). The quantity $I_{d\alpha}$ can be calculated with models like that proposed by Perez et al. (1990a) or can be derived from a measurement on the tilted plane (if available). The problem associated with the broadband normalization method is mainly a skewing of the spectrum because of not accounting for higher water-vapor and droplet absorption, which have been discussed in earlier investigations (Bird et al. 1987; Nann 1989a).

The quantity $R(\lambda)$ can now be calculated, making use of $E'_\alpha(\lambda)$, which has been normalized by the broadband measurements instead of the spectroradiometer reading at 630 nm:

$$R(\lambda) = \frac{\text{measurement}(\lambda)}{E'_\alpha(\lambda)}. \qquad (10)$$

The results in Fig. 10 compared with Fig. 4 show that the standard deviation $\sigma(\lambda)$ is only slightly reduced (except for the clear-sky situation) by using the spectrum calculated with SPCTRAL2 instead of the fixed ASTM standard spectrum as a reference. The mean of $R(\lambda)$, however, is closer to 1.0 than in Fig. 4. But it should be kept in mind that the normalization method no longer uses the spectroradiometer signal at 630 nm. To make Figs. 4 and 10 really comparable, the bias and standard deviations of Fig. 10 must be reduced by R (630 nm) and σ (630 nm). (The latter reduction might be slightly high because there are some uncorrelated measurement random errors.)

Obviously, for the clear-sky case the aerosol scattering and absorption is not treated well, as can be seen in Fig. 10c. As was discussed in section 3a, information about the amount and size distribution of aerosols is highly uncertain and is not very much improved by the visibility information (for the German site). This lack of information about the aerosol parameters limits all efforts concerned with spectral modeling. Furthermore, the deviations between the model and measurement under clear skies are strongly zenith correlated. This fact gives some evidence that the aerosol absorption and scattering (probably the ozone absorption too) are not treated exactly by the (single scattering) code SPCTRAL2 (for zenith angles greater than 65°). Similar comments were made by Olseth et al. (1989) (and Thomalla and Thamm, personal communication). This effect was investigated to see if it is caused by a cosine error of the spectroradiometer (angle of incidence related), but it is not.

b. Correction function CCM (λ, K_t)

According to the analysis in section 3, the deviations in Figs. 10a,b are caused mainly by the spectral influence of clouds, which can be corrected by a correlation equation with the clearness index as predictor variable. The normalized spectral irradiance $E'_\alpha(\lambda)$ was compared with the whole German dataset to derive the correction function CCM (λ, K_t). This so-called "cloud cover modifier" corrects mainly for the spectral cloud effects identified in section 4. CCM also corrects errors caused by SPCTRAL2 itself, as well as incorrect input data for water vapor aerosols, and ozone, or incorrect surface reflectance data (our model uses the spectral

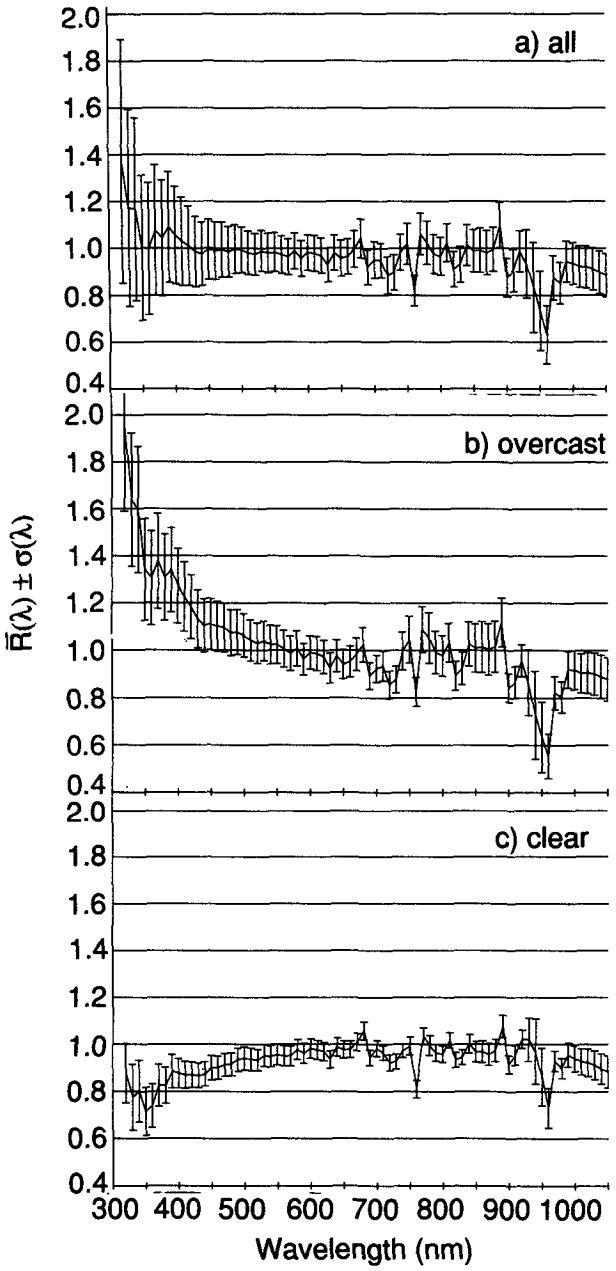

FIG. 10. The complete German dataset of spectral measurements (a) along with only overcast-sky (b) and clear-sky (c) measurements all divided by the normalized clear-sky simulation. Shown is the mean of $R(\lambda)$ and $\pm\sigma(\lambda)$ for each wavelength derived from Eq. (10) (broadband normalization).

reflectance of a vegetative surface cover). As discussed in section 2, the water-droplet absorption from clouds affects mainly the region beyond 1400 nm. Because we have no information on the liquid-water amount, the normalization method causes $E'_\alpha(\lambda)$ to be skewed when the liquid-water amount increases. This effect is compensated by CCM (λ, K_t) also. Of course, CCM also corrects for the measurement errors of all instruments, especially the spectroradiometer. The CCM is calculated using a polynomial fit (quadratic regression model) for all $R(\lambda)$ of Eq. (10):

$$\text{CCM}(\lambda, K_t) = A(\lambda) + B(\lambda)K_t + C(\lambda)K_t^2. \quad (11)$$

To improve the correlation A, B, and C, were calculated separately for summer and fall. [Note that for the overcast data sample in section 4a an exponential fit with two coefficients was sufficient, as shown in Eq. (7), Fig. 5, and Nann and Riordan (1990b).] The coefficients of Eq. (11), along with the standard deviation of the regression, are given in Fig. 11. The wavelength resolution is 10 nm, so one has an array consisting of 246 values.

Finally, Fig. 12 shows how the "predicted" irradiance $E'_\alpha(\lambda)\text{CCM}(\lambda, K_t)$ compares with the measured one. The overall standard deviation is about 8% in the VIS, up to 15% in the UV, and 18% around 940 nm at the water-vapor absorption band. The spread around 940 nm is partly caused by the sharp profile of the absorption band and resolution mismatch between model and measurement. Compared with Fig. 10, the CCM as a function of K_t has especially reduced the deviations in the UV and blue regions, where the cloud effects were largest. The performance of SEDES1 is very good for overcast-sky conditions where the standard deviation is only 7% in the VIS, and for clear-sky conditions where the standard error is 5% in the VIS.

c. An estimate for the NIR irradiance beyond 1050 nm

In spite of the high cosine response error of the device beyond 1050 nm, the CCM (λ, K_t) was also calculated in this region. To get an estimate for the spectral irradiance beyond 1100 nm (which according to Table

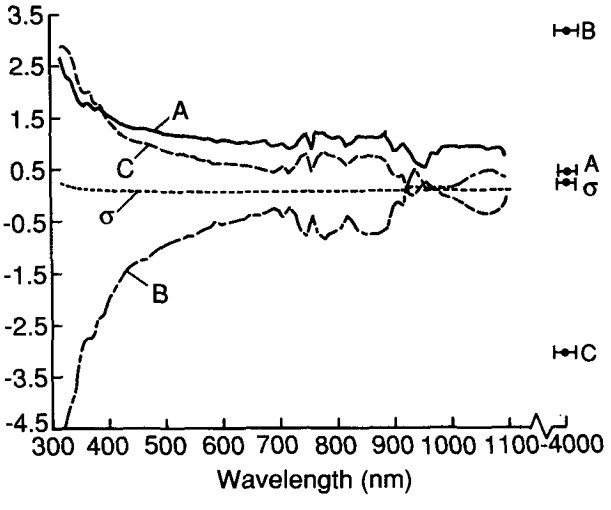

FIG. 11. Coefficients $A(\lambda)$, $B(\lambda)$, and $C(\lambda)$ of Eq. (11) for the whole German dataset and the standard deviation of the regression. Using $A(\lambda)$, $B(\lambda)$, and $C(\lambda)$ one can calculate the absolute spectral distribution with SEDES1. Also shown are the estimates for the 1100–4000 nm region.

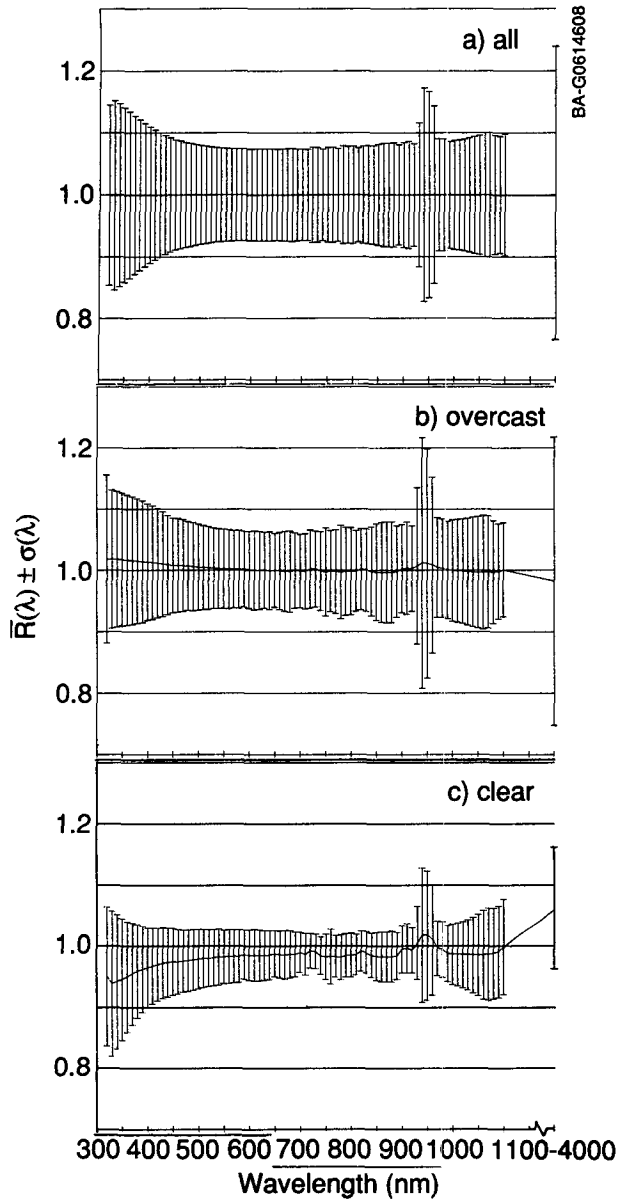

FIG. 12. Comparison of measurements and calculations with the new model SEDES1 for the whole dataset (a) overcast-sky data (b) and clear-sky data (c) at Stuttgart summer and fall 1989.

2 includes 22% of the incoming energy), the CCM (1100–4000 nm, K_t) was calculated from the difference between the integrated irradiance up to 1100 nm (spectroradiometer) and up to 4000 nm (pyranometer), divided by the normalized simulation between 1100 and 4000 nm. The results can be seen in Figs. 11 and 12.

6. Conclusions

Several thousand solar spectra were recorded, along with the major meteorological and solar irradiance observations at four sites over several months. In comparing the measurements with the ASTM standard spectrum and a clear-sky simulation, a correlation was found between the clearness index K_t (representing the cloud optical thickness τ) and the relative spectral transmission of clouds. It was shown that the measurement uncertainty (section 3) is less than the magnitude of the effects observed. The measured cloud effects (higher relative transmission in the UV and blue regions, albedo enhancement, and increased water-vapor absorption) could be qualitatively understood from previous studies and the Paris cloudy-sky model (section 2). The relative transmission under cloudy skies in the UV and blue regions, however, is higher than expected from theory. This result is supported by previous investigations using a different data analysis approach (Nann and Riordan 1990b) and other studies (Paris and Justus 1988; Bird et al. 1987; Elhadidy et al. 1990). Perez et al. (1990a) found an exponential increase of the luminous efficiency under overcast skies with a decreasing K_t similar to our result. However, their explanation that this effect is mainly caused by the increased water-vapor (and droplet) absorption is not sufficient. As was shown in section 4, using the normalization at 630 nm, the relative higher transmission for shorter wavelengths under overcast skies does not result from simply skewing the spectrum.

We proposed a semiempirical model SEDES1 to predict global spectral irradiance under clear and cloudy skies. SEDES1 (see Fig. 9) is based on the clear-sky approximation model SPCTRAL2 and a cloud cover modifier CCM. Using global and diffuse irradiance, water vapor, and the sun's position as the input data, SEDES1 predicts the measured spectrum between 320 and 1050 nm with a standard deviation between 8% and 18% for all sky conditions. SEDES1 cannot be used to calculate the direct and diffuse spectral irradiance separately unless detailed information on the aerosol particle distribution and amount is available.

However, this approach using the CCM also corrects all systematic errors, including bias measurement errors. Therefore, SEDES1 shows bias errors of at least the same magnitude as the spectroradiometer's bias errors. The standard deviations in Fig. 12 are close to the overall random error uncertainty of our system, which is mainly composed of the random errors of Table 1 plus the ±5% fluctuations allowed by the total irradiance stability check during the spectral scan. This supports the hypothesis that the variability in the spectral irradiance caused by clouds, aerosols, and water vapor (which is not explained by SEDES1) is about 6% (estimated from the root-mean-square of all three components).

We can conclude that the variations of the total spectral irradiance on a tilted surface may be inferred with reasonable precision for clear- and cloudy-sky conditions from the knowledge of two radiative quantities (direct and diffuse irradiance), the sun's position, and water vapor. This point is made because the vari-

ability of the spectral irradiance appeared to be predictable, even considering the wide range of possible cloud types, heights, and distribution. In similar investigations, Perez et al. (Perez 1990a) developed a semiempirical model for daylight availability and also found that these four quantities are sufficient to describe the radiative transfer properties as measured with the precision of the given instrumentation and under the restriction of easily available input data.

Future work, however, must determine whether the empirically derived CCM (λ, K_t) is appropriate for cases other than the German site, measurement techniques, and periods before any final conclusion can be drawn. Adjustments are likely because of the site- and climate-dependent characteristics of clouds; the performance of the water-vapor and aerosol approximations; and the specific characteristics of our instruments, tilt angle, and ground cover. Two long-term and improved experiments operated by the Centre for Solar Energy and Hydrogen Research (ZSW) address this question. Also, we expect that the CCM could be improved by including other readily accessible variables in addition to K_t to the functional form of the CCM.

The semiempirical model SEDES1 now allows us to calculate different representative spectra for different atmospheric conditions. Examples of these representative spectra, calculated using clearness indices from 0.1 to 0.8, are shown in Fig. 13. The model can also be applied to predict the total spectral irradiance in short-time steps (30 or 60 minutes) for clear, partly cloudy, and overcast conditions.

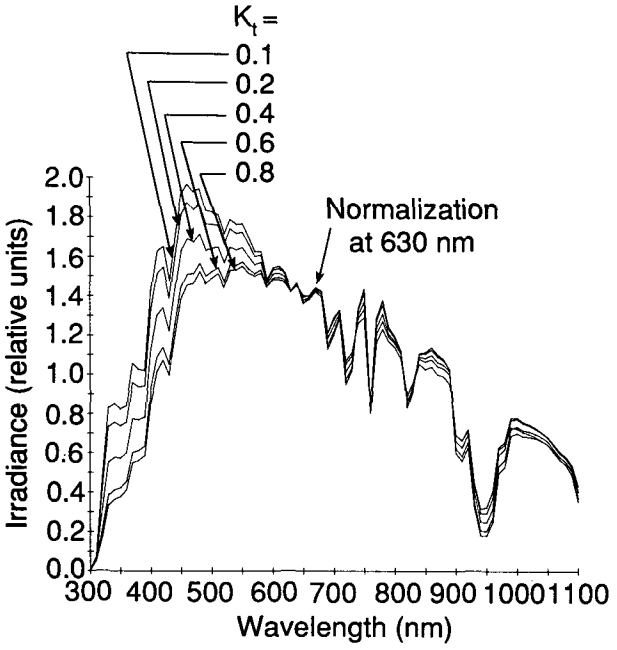

FIG. 13. Typical spectra calculated with SEDES1. The geometry is fixed for a zenith angle of 48° and normal incidence; aerosol optical depth is 0.23, and precipitable water vapor is 1.73 cm; K_t determines all other irradiance parameters as they occured for a given K_t on average for the German site.

Acknowledgments. The authors wish to express their thanks to Dr. C. F. Bohren (Pennsylvania State University), Dr. C. G. Justus (Georgia Institute of Technology), and Dr. R. Perez (State University of New York at Albany) for their essential and very constructive comments. Dr. Bohren added valuable insights to the discussion in section 2. The authors would like to acknowledge R. Schelp (ZSW) for acquiring the German data; W. Marion at the Florida Solar Energy Center, C. Jennings and C. Whitaker at the Pacific Gas and Electric Company, and T. Stoffel at SERI for acquiring the United States data; and D. Myers at SERI for data processing and instrument calibration support. Lastly, we offer a word of gratitude to Prof. Dr. W. H. Bloss, and R. L. Hulstrom whose guidance made this research possible.

REFERENCES

Bird, R. E., and C. Riordan, 1986: Simple solar spectral model for direct and diffuse irradiance on horizontal and tilted planes at the earth's surface for cloudless atmospheres. *J. Climate Appl. Meteor.*, **25**, 87–97.

——, —— and D. R. Myers, 1987: Investigation of a cloud cover modification to SPCTRAL2. TR-215-3038,

Bohren, C. F., 1987: Multiple scattering of light and some of its observable consequences. *Amer. J. Phys.*, **55**, 524.

——, 1990a: Colors of the sky: New light on an old problem, SPIE meeting, Orlando, 18 April 1990.

Bolsenga, S. J., 1965: The relationship between total atmospheric water vapor and surface dewpoint on a mean daily and hourly basis. *J. Appl. Meteor.*, **4**, 430–432.

Brest, C. L., 1987: Seasonal albedo of an urban/rural landscape from satellite observations. *J. Climate Appl. Meteor.*, **26**, 1169–1187.

Elhadidy, M. A., D. Y. Abdel-Nabi and P. D. Kruss, 1990: Ultraviolet solar radiation at Dhahran, Saudi Arabia. *Solar Energy*, **44**, 315.

Eltermann, L., 1970: Relationship between vertical attenuation and surface meteorological range. *Appl. Optics*, **9**, 1804.

Garrison, J. D., and P. Adler, 1990: Estimation of precipitable water over the United States for application of the division of solar radiation into its direct and diffuse components. *Solar Energy*, **44**, 225.

Hulstrom, R., R. Bird and C. Riordan, 1985: Spectral solar irradiance datasets for selected terrestrial conditions. *Solar Cells*, **15**, 365.

Kasten, F., 1980: A simple parameterization of the pyrheliometric formula for determining the Linke turbidity factor. *Meteor. Rundsch.*, **33**, 124.

——, K. Dehne and W. Brettschneider, 1983: Improvement of measurement of diffuse solar radiation. *Solar Radiation Data*, W. Palz, ed., D. Reidel Publishing, 221–225.

Koschmieder, H., 1924: Theorie der horizontalen Sichtweite. *Beitraege Physik Atmosphaere*, **12**, 33–171.

Kriebel, K. T., 1978: On the determination of the atmospheric optical depth by measurements of the meteorological range. *Beitraege Physik Atmosphaere*, **51**, 330.

Leckner, B., 1978: The spectral distribution of solar radiation at the earth's surface—elements of a model. *Solar Energy*, **20**, 143.

Love, P. K., 1988: Bulk radiative characteristics of homogeneous water clouds at solar wavelengths. Ph.D. thesis, University of Wellington, New Zealand, 199 pp.

McClatchey, R. A., and J. E. Selby, 1972: Atmospheric Transmittance from 0.25 to 38.5 μm: Computer Code LOWTRAN-2. AFCRL-72-0745, Environ. Res. Paper 427,

Middleton, W. E. K., 1954: The color of the overcast sky. *J. Opt. Soc. Am.*, **44,** 793.

Myers, D. R., 1989: Estimates of uncertainty of measured spectra in the SERI spectral solar radiation database. *Solar Energy,* **43,** 347.

Nann, S., 1989a: Modeled and measured solar spectral irradiance for solar spectral energy applications under cloudy skies. *Proc. Daylight and Solar Radiation Symposium,* Technische Universitaet Berlin, Commission International De L'Eclairage and World Meteorological Organization, 108 pp.

——, 1989b: Uncertainties in determination of short-circuit current from measured and modeled spectral solar irradiance. *Proc. 9th European PV Solar Energy Conf.,* Commission of European Countries, Freiburg, 204.

——, 1990a: A cloud cover modifier for solar spectral irradiance modeling. *Proc. ISES Solar World Congress,* International Solar Energy Society, Kobe, in press.

——, and C. Riordan, 1990b: Solar spectral irradiance under overcast skies. *Proc. 21st IEEE PV Spec. Conf.,* Institute of Electrical and Electronic Engineers, Inc., Orlando, 1110–1115.

Olseth, J. A., and A. Skartveit, 1989: Observed and modeled hourly luminous efficacies under arbitrary cloudiness. *Solar Energy,* **42,** 221.

Paris, M. V., 1985: Model studies of solar spectral irradiance at the bottom and top of a cloudy atmosphere. Ph.D. thesis, Georgia Institute of Technology, Atlanta, 135 pp.

——, and C. G. Justus, 1988: A cloudy-sky radiative transfer model suitable for calibration of satellite sensors. *Remote Sens. Environ.,* **26,** 269.

Perez, R., P. Ineichen, R. Seals, J. Michalsky and R. Stewart, 1990a: Modeling daylight availability and irradiance components from direct and global irradiance. *Solar Energy,* **44,** 271.

——, ——, ——, —— and ——, 1990b: Making full use of the clearness index for parameterizing hourly insolation conditions. *Solar Energy,* **45,** 111.

Peterson, J. T., and C. J. Fee, 1981: Visibility-Atmospheric turbidity dependence at Rayleigh, *Atmos. Environ.,* **15,** 2561–2563.

Powell, M. Jr., 1986: A simple solar spectral model studying the effect of cloud cover and surface albedo on the incoming solar radiation. Ph.D. thesis, The University of Michigan, Ann Arbor,

Reitan, C. H., 1963: Surface dewpoint and water vapor aloft. *J. Appl. Meteor.,* **2,** 776–779.

Riordan, C., et al., 1989: Spectral solar radiation data base at SERI. *Solar Energy,* **42,** 67.

Shine, K. P., 1984: Parameterization of the shortwave flux over high albedo surfaces as a function of cloud thickness and albedo. *Quart. J. Roy. Meteor. Soc.,* **110,** 767.

Smith, W. L., 1966: Note on the relationship between total precipitable water and surface dewpoint. *J. Appl. Meteor.,* **5,** 726–727.

Tomasi, C., 1981: Determination of the total precipitable water by varying the intercept in Reitan's relationship. *J. Appl. Meteor.,* **20,** 1058–1069.

——, 1982: Feature of the scale height for particulate extinction in hazy atmospheres. *J. Appl. Meteor.,* **21,** 931.

Volz, F. E., 1969: Some results of turbidity networks. *Tellus,* **21,** 625.

Welch, R. M., S. K. Cox and J. M. Davis, 1980: Solar radiation and clouds. *Meteor. Monographs,* **17,**

Wiscombe, W. J., and R. M. Welch, 1986: Reply to comments on the effects of very large drops on cloud absorption. Part I: Parcel methods. *J. Atmos. Sci.,* **43,** 401–407.

——, R. M. Welch and W. D. Hall, 1984: The effects of very large drops on cloud absorption. *J. Atmos. Sci.,* **41,** 1336.

Wright, J., R. Perez and J. J. Michalsky, 1989: Luminous efficacy of direct irradiance: Variations with insolation and moisture conditions. *Solar Energy,* **42,** 387.